NIH Public Access
Author Manuscript
J Polym Sci A Polym Chem. Author manuscript; available in PMC 2013 January 01.

Published in final edited form as:
J Polym Sci A Polym Chem. 2012 January 1; 3(11): 3146–3156. doi:10.1039/C2PY20324C.

pH-Triggered reversible morphological inversion of orthogonally-addressable poly(3-acrylamidophenylboronic acid)-*block*-poly(acrylamidoethylamine) micelles and their shell crosslinked nanoparticles

Jiong Zou[a], **Shiyi Zhang**[a,b], **Ritu Shrestha**[a], **Kellie Seetho**[a], **Carrie L. Donley**[c], and **Karen L. Wooley**[a]

Karen L. Wooley: wooley@chem.tamu.edu

[a]Departments of Chemistry and Chemical Engineering, Texas A&M University, P.O. BOX 30012, 3255 TAMU, College Station, Texas, 77842, (USA)

[b]Department of Chemistry, Washington University in St. Louis, St. Louis, Missouri, 63130, (USA)

[c]Chapel Hill Analytical and Nanofabrication Laboratory Institute for Advanced Materials, University of North Carolina 243 Chapman Hall, Chapel Hill, North Carolina, 27599, (USA)

Abstract

Functionally-responsive amphiphilic core-shell nanoscopic objects, capable of either complete or partial inversion processes, were produced by the supramolecular assembly of pH-responsive block copolymers, without or with covalent crosslinking of the shell layer, respectively. A new type of well-defined, dual-functionalized boronic acid- and amino-based diblock copolymer poly(3-acrylamidophenylboronic acid)$_{30}$-*block*-poly(acrylamidoethylamine)$_{25}$ (PAPBA$_{30}$-*b*-PAEA$_{25}$) was synthesized by sequential reversible addition-fragmentation chain transfer (RAFT) polymerization and then assembled into cationic micelles in aqueous solution at pH 5.5. The micelles were further cross-linked throughout the shell domain comprised of poly(acrylamidoethylamine) by reaction with a bis-activated ester of 4,15-dioxo-8,11-dioxa-5,14-diazaoctadecane-1,18-dioic acid, upon increase of the pH to 7, to different cross-linking densities (2%, 5% and 10%), forming well-defined shell cross-linked nanoparticles (SCKs) with hydrodynamic diameters of *ca.* 50 nm. These smart micelles and SCKs presented switchable cationic, zwitterionic and anionic properties, and existed as stable nanoparticles with high positive surface charge at low pH (pH = 2, zeta potential ~ +40 mV) and strong negative surface charge at high pH (pH = 12, zeta potential ~ −35 mV). ^{1}H NMR spectroscopy, X-ray photoelectron spectroscopy (XPS), dynamic light scattering (DLS), transmission electron microscopy (TEM), atomic force microscopy (AFM), and zeta potential, were used to characterize the chemical compositions, particle sizes, morphologies and surface charges. Precipitation occurred near the isoelectric points (IEP) of the polymer/particle solutions, and the IEP values could be tuned by changing the shell cross-linking density. The block copolymer micelles were capable of full reversible morphological inversion as a function of pH, by orthogonal protonation of the PAEA and hydroxide association with the PAPBA units, whereas the SCKs underwent only reptation of the PAPBA chain segments through the crosslinked shell of PAEA as the pH was elevated. Further, these nanomaterials also showed D-glucose-responsive properties.

Correspondence to: Karen L. Wooley, wooley@chem.tamu.edu.

[†]Electronic Supplementary Information (ESI) available: [DLS Zeta potential and XPS characterization of non-cross-linked micelles and czaSCKs as a function of pH and concentration D-glucose]. See DOI: 10.1039/b000000x/

Introduction

During the past decade, “smart” or “intelligent” stimuli-responsive polymers have attracted increasing research interest because of the change of their morphologies, surface charges and properties upon external stimuli, such as pH, temperature, light, salt concentration and the combination of these parameters.[1–7] Nanoscopic materials derived from stimuli-responsive block copolymers have broad potential for applications in a variety of areas, including switches and sensors,[8, 9] drug delivery vehicles,[10–12] diagnostics[13] and antifouling coatings.[14] The most simple and common examples of smart block copolymer nanostructures are conventional micelles composed of AB diblock copolymers, which in aqueous media form A-B, core-shell morphologies, having A in the core and B in the shell. In 2002, Liu and Armes reported the first example of pH-responsive zwitterionic diblock copolymers that underwent reversible switching between the two micellar states A-B, core-shell micelles vs. B-A, core-shell reverse micelles at ambient temperature, solely by adjusting the solution pH.[15, 16] Further, Armes and co-workers pioneered several techniques to construct smart micelles that responded to pH, temperature and salt concentration and named them as “schizophrenic” polymers.[17, 18] Our group also developed pH-induced reversible assembly of micelles from poly(acrylic acid)-b-poly(p-hydroxystyrene) (PAA-b-PpHS).[19] Besides micelles, pH-triggered reversible vesicles have also been reported by Eisenberg’s[20] and Lecommandoux’s groups,[21] respectively. It has been well established that the cross-linking of micelles can both stabilize the nanostructures and also tune the properties of assembled micelles.[22, 23] However, only few papers have reported cross-linked ‘schizophrenic’ micelles,[24, 25] although without detailed studies on how the cross-linking affected the properties and morphologies of those micellar assemblies.

Among several stimuli-responsive polymers, those containing boronic acid-functionalized repeat units are of particular interest because of their potential applications as sensor materials,[26] self-regulated insulin delivery systems,[27] and flame-retardant materials.[28] Stimuli-responsive micelles comprised of block polymers with boronic acid functionalities have been reported by Sumerlin and coworkers.[29–31] In their system, triple responsiveness was generated by the boronic acid-containing block segment responding to pH and glucose stimuli, along with a thermally-responsive poly(N-isopropylacrylamide) block segment. However, the micelles or reverse micelles were limited to negative or neutral surface charges. In this paper, we demonstrate a new type of diblock copolymer composed of poly(3-acrylamidophenylboronic acid)-*block*-poly(acrylamidoethylamine) (PAPBA-*b*-PAEA), **1**, and investigate the pH-driven morphological inversion behaviors for its nanoscopic polymer micelle assemblies and shell crosslinked nanoparticles, with possibilities for cationic, zwitterionic and anionic surface charges. By taking advantage of the significant hydrophobic to hydrophilic change of the boronic acid-containing blocks with elevation of the pH, and hydrophobic to hydrophilic change of the amino-containing blocks of PAEA upon protonation at low pH, this block copolymer undergoes assembly in aqueous solution to form orthogonally-addressable core-shell or shell-core micelles having either an anionic surface and a PAEA core at high pH or a cationic surface and a PAPBA core at low pH, respectively. The micelles were further cross-linked throughout the shell domain with different cross-linking degrees, resulting in cationic-zwitterionic-anionic shell-cross-linked knedel-like nanoparticles (czaSCKs), where the surface charge transitions are pH tunable. The pH triggered inside-out change of both the czaSCKs and the non-cross-linked micelles were observed to be reversible, although the topological difference for a supramolecular micellar assembly of polymer chains is quite different from the czaSCK unimolecular nanostructure having the core chains fixed to a crosslinked shell. Further, the isoelectric point (IEP) of czaSCKs could be tuned by using different cross-linking densities. These smart czaSCKs with tunable IEP have potential for application as nanoscopic devices for protein separation and purification, metal ion enrichment and recovery from wastewater or

polluted soils, as metal catalyst supports for organic reactions,[32] among others. For instance, sensor applications could arise from the ability of the boronic acid units to bind with diol-containing compounds (*e.g.* D-glucose) with high affinity through reversible boronic ester formation, and the smart czaSCKs and micelles showed glucose-responsive property.

Results and Discussion

Synthesis and Characterization of $PAPBA_{30}$-*b*-$PAEA_{25}$

The synthesis of boronic acid-containing polymers has been conducted primarily by conventional radical polymerization or post-modification strategies.[27, 33] Uncontrolled conventional radical polymerization usually results in ill-defined copolymers or cross-linked gels, while incomplete chemical transformation efficiencies limit the ability of post-modification methods to produce highly-functionalized block copolymers. However, well-defined boronic acid block (co)polymers have been synthesized by controlled radical polymerizations (CRP), including atom transfer radical polymerization (ATRP)[34, 35] and reversible addition-fragmentation chain transfer (RAFT)[36] polymerization.

In this paper, the dual boronic acid- and amino-functionalized diblock copolymer **1**, was synthesized in three steps, by two sequential RAFT polymerizations and a deprotection (Scheme 1). The first step involved RAFT polymerization of (3-acrylamidophenyl)boronic acid (APBA, **2**) to construct the first block (PAPBA, **3**) by using 2,2′-azobis(isobutyronitrile) (AIBN) as radical initiator and 2-dodecylsulfanylthiocarbonylsulfanyl-2-methylpropionic acid (DDMAT, **4**) as chain transfer agent (CTA) with the feed ratio of $[APBA]_0 : [DDMAT]_0 : [AIBN]_0 = 50 : 1 : 0.2$. The polymerization was conducted at 70 °C in DMF/water mixture (95/5, v/v) and reached 70% conversion after 7 h, which was confirmed by ^{1}H NMR spectroscopy.

The small amount of water was necessary to prevent cross-linking *via* boroxine formation. The boronic acid polymer could not be directly characterized by gel permeation chromatography (GPC) analysis because of its limited solubility. By using pinacol protection on the boronic acid functionality, the polymer became soluble in DMF. The GPC analysis showed that the protected PAPBA **3** exhibited a monomodal molecular weight distribution with a polydispersity index (PDI) of 1.08 (Figure 1). The number-average molecular weight calculated by ^{1}H NMR spectroscopy was 6.2 kDa with $DP_n = 30$. The resulting homopolymer PAPBA **3** served as a macro-CTA for sequential RAFT polymerization of *tert*-butyl(2-acrylamidoethyl)carbamate (AEANBoc, **5**) with a feed ratio of $[\mathbf{5}]_0 : [\mathbf{3}]_0 : [AIBN]_0 = 50 : 1 : 0.2$, as the second step. The polymerization was conducted at 70 °C in DMF/water mixture (98/2, v/v) and reached 65% conversion in a period of 8 h. The crude mixture was purified by precipitation into cold diethyl ether to give the product diblock copolymer **6** as a pale yellow solid in 85% yield. GPC analysis showed a shift in the retention time from 24.1 min to 22.6 min, on chain extension from **3** to **6**, respectively, with maintenance of the monomodal molecular weight distribution and PDI = 1.10 for pinacol-protected **6** (Figure 1). The controlled polymerization was also supported by the experimental molecular weight as measured by ^{1}H NMR spectroscopy ($M_{n,NMR}$ = 11.6 kDa, $(DP)_{PAEANBoc} = 25$) being consistent with the theoretical molecular weight of 12.6 kDa. After removal of the Boc protecting groups by trifluoroacetic acid (TFA), the dual-functionalized block copolymer **1** was obtained. The crude product was purified by dialysis against nanopure water for 2 d to remove residual TFA and was then lyophilized.

Characterization of pH and D-glucose dual responsive micelles and czaSCKs

The opposing and individually-addressable pH-responsive characteristics of the phenylboronic acid and amino groups were utilized to drive the assembly into reversible

nanoscopic micellar structures having either anionic boronate-functionalized polymer shells with neutral amino-functionalized polymer segments in the core at high pH values, or cationic ammonium-functionalized polymer shells and neutral boronic acid polymer cores at low pH values; under intermediate pH conditions, zwitterionic polymer chains gave ill-defined and large aggregates. In aqueous solution, boronic acid-containing compounds have unique pH-responsive properties, due to the equilibrium between the uncharged and negatively-charged forms of the boronic acid functionality. Above the pK_a of the phenylboronic acid (pK_a ~ 9), most of the boronic acids on PAPBA form tetrahedral boronates with hydroxide in water, which results in hydrophilic boronate polyanionic polymers. When acidified to pH below the pK_a, the boronate moieties convert back to neutral hydrophobic boronic acid groups and subsequent chain dehydration occurs. The PAEA block presents opposite pH-responsive properties, giving hydrophilic protonated ammonium groups at pH below the pK_a ~ 9.1 and relatively hydrophobic neutral amines at high pH (Scheme 2). The self assembly of the diblock copolymers into micelles was conducted at room temperature by directly dissolving the polymer PAPBA$_{30}$-*b*-PAEA$_{25}$ in nanopure water at pH 5.5, followed by sonication for 5 min. Based on the block composition, micelles with PAPBA within the cores and PAEA comprising the shells were expected to form at low pH, and reverse micelles with PAEA cores and PAPBA shells at high pH. Importantly, the pH-triggered micellar assembly and its cyclical reversion as a function of increasing and decreasing the pH were studied as dynamic supramolecular micelle nanostructures *vs.* their covalent PAEA-shell crosslinked analogs. Dynamic light scattering (DLS), ^{1}H NMR spectroscopy, X-ray photoelectron spectroscopy (XPS), zeta potential, transmission electron microscopy (TEM), and atomic force microscopy (AFM) were used to characterize the size, chemical composition, surface charge and morphology of the assembled nanoparticles.

^{1}H NMR spectroscopy, a widely-used and powerful technique to characterize the chemical composition and morphology of micelles, was applied to investigate the micellar assembly and inversion processes, without and with shell crosslinking. D_2O was used to prepare micelles with the polymer concentration of 1.0 mg/mL and the solution pH was tuned with deuterium chloride (DCl) and sodium deuterium oxide (NaOD). The resulting micelle solutions were directly transferred to NMR tubes for ^{1}H NMR measurements. As shown in Figure 2, under acidic conditions (pH = 2), the methylene proton signals on the PAEA block, resonating at 3.20 and 3.53 ppm, can be clearly observed, whereas a measurable signal for the aromatic protons of the phenylboronic acids on the PAPBA block is lacking. This result indicates that the PAEA block was solvated in D_2O and gave strong signals, whereas the hydrophobic PAPBA block was embedded in the core and poorly solvated. On the contrary, under basic conditions (pH = 12), the integration of the methylene proton signals on the PAEA block at 2.73 and 3.23 ppm is lower than the aromatic protons on the PAPBA block around 6.3–7.5 ppm, which can be attributed to the formation of reverse micelles with PAPBA as the solvated shell chain segments and PAEA packaged within the core domain. The micelles were then cross-linked throughout the PAEA shell domains at pH 7–8 by using 4,15-dioxo-8,11-dioxa-5,14-diazaoctadecane-1,18-dioic acid as the cross-linker, and N-hydroxybenzotriazole (HOBt) and 2-(1H-benzotriazole-1-yl)-1, 1, 3, 3-tetramethylaminium hexafluorophosphate (HBTU) as condensation reagents.[21] The czaSCKs were obtained with different cross-linking degrees (2%, 5% and 10%, based upon the stoichiometric ratios of cross-linker *vs.* initial theoretical amine residues, *i.e.* 0.01 eq, 0.025 eq, and 0.05 eq, respectively). The czaSCK solutions were lyophilized and resuspended into D_2O solutions with the pH adjusted to desired values by DCl and NaOD additions. As expected, at pH 2, the czaSCKs cross-linked at higher density showed lower shell proton signals than did the czaSCKs cross-linked to a lower extent or the non-cross-linked micelles.

Zeta potential (ζ) measurements were used to study the surface charges of the dynamic micellar polymer assemblies as a function of pH. As shown in Figure 3, micelles prepared at pH 2 without cross-linking showed high positive surface charge, *ca.* +37 mV. NaOH (0.1 M) was added to the micelle solution to tune the pH and then zeta potential measurements were followed. The ζ increased from +37 mV to +51 mV during the pH change from 2.0 to 5.1, and then continuously dropped from +51 mV (pH = 5.1) to −22 mV (pH = 12.0), giving an isoelectric point (IEP, ζ = 0) at 9.52. At low pH (pH<6), cationic conventional micelles were produced, in which the primary amine groups on the PAEA blocks were protonated to form hydrophilic shells while the hydrophobic PAPBA comprised the core domains. Anionic reverse micelles formed at high pH (pH>10.5), with hydrophilic boronic acid hydroxide PAPBA as the shells and deprotonated PAEA as the cores. Then, 0.1 M of HCl was added to decrease pH from 12.0 to 3.2 with monitoring by zeta potential measurements. Interestingly, the surface charge values and the IEP at 9.59 were similar to the data obtained from the experiments that involved change from acidic to basic conditions, indicating cyclical reversibility for the assembly processes.

The pH-responsive particle size changes of the polymer micelles were studied by using DLS. As shown in Figure 4, with an increase of pH, the volume-based hydrodynamic diameter ($(D_h)_v$) remained constant at *ca.* 70 nm over a range of pH 2~6, with monomodal distributions, and the sample appeared as a bluish micelle solution (Figure S1). With further increasing pH (from 6 to 8), the solution became turbid, and DLS showed bimodal distributions (Figure S1) with large metastable aggregates ($(D_h)_v$ *ca.* 330 nm) and small particles ($(D_h)_v$ *ca.* 50 nm). A large amount of precipitates appeared over the IEP region (pH 8.0~10.2, shadowed part in Figure 4), which is expected to be due to electrostatic attractions of the partially-positive PAEA and partially-negative PAPBA causing reorganization within micelles and micelle-micelle interactions to result in macroscopic particle growth. With further elevation of the pH, large reverse micelles ($(D_h)_v$ *ca.* 80~100 nm, pH *ca.* 10.5) and then small reverse micelles ($(D_h)_v$ ~5 nm, pH>12) were observed. At high pH, hydroxide ions entered into the cores, bound boronic acid functional groups *via* dynamic covalent bonds to form tetrahedral boronates, which converted the hydrophobic boronic acid polymer block (PAPBA) to hydrophilic boronate polyanion, resulting in anionic reverse micelles having PAPBA as the shells and PAEA as cores. The hydrodynamic size change of micelles was reversible when decreasing pH from 12 to 2.

The czaSCKs with different levels of cross-linking density were also characterized by zeta potential and DLS as a function of pH (Figure 5). With 2 % cross-linking density, the czaSCKs prepared at pH 2 had positive zeta potential, *ca.* +45 mV, which was similar to the non-cross-linked micelles. The zeta potential remained constant during the pH change from 2.0 to 7.4 and then dropped gradually from +46 mV (pH 7.4) to −33 mV (pH 11.6). The IEP of the 2 % cross-linked czaSCKs, obtained during acidic to basic solution pH change was 10.16, which was higher than was observed for the non-cross-linked micelles (IEP = 9.59). The zeta potential values were also plotted as a function of pH with the reverse pH transition from basic to acidic conditions. The surface charge values were similar to the data obtained from the experiments that involved change from acidic to basic conditions, however the IEP obtained from basic to acidic pH change was 9.51, which was similar to the IEP of non-cross-linked micelles. The ability to transition reversibly from cationic to anionic surface charge on elevation of the pH and then anionic to cationic on return to acidic conditions indicates reversible morphological changes, which for these czaSCKs was expected to proceed by PAPBA chain reptation from the core through the shell to the surface and back into the core, respectively. The DLS measurements indicated that the $(D_h)_v$ was constant ~ 90 nm during the pH change from 2.0 to 8.6, followed by precipitate formation over the IEP region (pH 8.7 ~ 10.4), and return to a clear solution and uniform nanoscopic particles, $(D_h)_v$ ~ 92 nm, with further increase of the pH. The cross-linker in the shell provided stability and

confinement of the polymer chains within the nanoscopic assemblies, which resulted in diminished global disassembly and reassembly processes, while still allowing intra-particle reorganization events; compared to the non-cross-linked micelles, the czaSCKs did not form metastable large aggregates immediately below the IEP and did not become very small assemblies at high pH values. By decreasing the pH, DLS results indicated that the inverted anionic SCK nanoparticles that had formed at pH 11.3 with $(D_h)_v$ = 75 nm transformed into cationic SCKs on reduction of the pH to 2.6 with $(D_h)_v$ ~ 45 nm. Similar zeta potential and DLS measurements as a function of pH were also conducted on 5 and 10 % cross-linked czaSCKs. For the 5 % cross-linked czaSCKs, the IEP values were 9.78 and 9.51, obtained by increasing and decreasing pH, respectively. DLS measurements of 5 % and 10 % cross-linked czaSCKs showed similar trends of hydrodynamic diameter changes as observed for the 2 % cross-linked czaSCKs, upon both acidic-to-basic and basic-to-acidic changes. With elevating pH, the IEP of 10 % cross-linked czaSCKs was 9.86 and with decreasing pH, IEP was 9.54. The hystereses with the data and the shifts of the IEPs for each of the cza SCKs to higher values during the elevating pH measurements are expected to be due to the crosslinked shell inhibiting progression of the PABPA chains from the particle core to its surface.

Transmission electron microscopy (TEM) was utilized to probe the size and morphology changes of non-cross-linked micelles and czaSCKs (Figure 6). The TEM-measured number-average diameter (D_{av}) of the micelle core domains was 43 ± 6 nm, which was in accordance with the DLS hydrodynamic diameter result ($(D_h)_v$ = 68 nm), taking into account the shell layer. The agreement of TEM and DLS diameter data and the circular two-dimensional particle images by TEM indicated that the micelles retained a spherical morphology on deposition from water onto the carbon-coated copper grid. At pH = 7.3, a combination of irregular aggregates and spherical nanostructures were observed, further supporting the micellar disassembly and reaggregation to form metastable intermediates that had been determined by DLS and zeta potential studies. At high pH 10.5, spherical micelles with a relatively broad size distribution D_{av} = 38 ± 12 nm were observed by TEM. Although DLS had observed assemblies of *ca.* 5 nm at pH 12, no micellar particles could be found in TEM observations. In contrast, the 2 % czaSCKs showed D_{av} = 39 ± 6 nm at pH 2 and retention of nanoscopic objects having D_{av} = 25 ± 3 nm at pH 12, again demonstrating the reinforcement of the nanoparticulate structure by the presence of the shell crosslinks. Similarly, the 5 % czaSCKs had D_{av} = 42 ± 4 nm at pH 2 and D_{av} = 35 ± 3 nm at pH 12; 10 % czaSCKs had D_{av} = 51 ± 9 nm at pH 2 and D_{av} = 44 ± 6 nm at pH 12. Tapping-mode AFM measurements of 10 % czaSCKs were also collected after deposition of samples at solution pH 2 and pH 12 onto freshly-cleaved mica and allowing them to dry under ambient conditions. In pH 2, for the 10 % czaSCKs, AFM presented well-defined round particles with *ca.* 160 nm diameter and 25 nm height (Figure 7a). In pH 12, particles with *ca.* 230 nm in diameter and 18 nm height were observed for the 10 % czaSCKs (Figure 7b). Relative to the carbon surface used for TEM, the highly polar mica surface led to significant collapse of czaSCKs on the substrate, and thus caused the particles to show larger than expected diameters and smaller than expected heights.

The glucose responsive studies were also conducted. Boronic acid and its derivatives are known to form reversible dynamic covalent complexes with cis-diol units such as D-glucose. The interaction between D-glucose and boronic acid is also pH sensitive. In aqueous media, boronic acid compounds exist in equilibrium between the charged (high pH) and uncharged (low pH) forms. The charged forms have much higher combination constant than the uncharged forms to make a stable complex with glucose through reversible dynamic covalent bonding.[22] To two samples of micelle solutions at pH 2, 5 equivalents and 15 equivalents of D-glucose compared to phenylboronic acid functionalities were added, respectively. Zeta potential values were measured and plotted as a function of pH (Figure 8).

In both 5 eq D-glucose and 15 eq D-glucose solutions, with increase of pH from 2 to 12, the IEP dropped to 8.91 (5 eq) and 8.86 (15 eq), respectively. With decrease of pH from 12 to 2, lower IEPs were obtained (8.60 (5 eq) and 8.05 (15 eq)). The drop of IEP indicated the successful incorporation between phenylboronic and D-glucose. With the formation of phenylborate, the pKa dropped from 9.0 to 6.8[22] on the boronic acid block, which resulted in the IEP drop for the entire micelle solutions. The 10 % cross-linked czaSCKs also exhibited similar IEP drop (8.00 (from acidic to basic change), 8.21 (from basic to acidic change) with existence of 15 eq of D-glucose) (Figure S2). DLS measurements were also conducted to monitor the size change of non-cross-linked micelles and 10 % czaSCKs as a function of pH with the existence of D-glucose (Figure S3). The size of micelles and czaSCKs in both low pH and high pH solutions remained constant, compared to the solutions without D-glucose. However the IEP regions for D-glucose containing systems were broader, compared to the D-glucose free systems, which may be due to hydrophilicity changes upon formation of the boronic acid D-glucose complexes.

XPS analysis of micelles and czaSCKs

The elemental analysis of micelles as well as czaSCKs by XPS were also carried out and the results are shown in Table 1 and Figures S4 and S5. XPS samples were prepared as follows: non-cross-linked micelle (2 mg/mL) or czaSCK (2 mg/mL, with 2%, 5% and 10% cross-linking densities) solutions prepared at pH 2 were deposited onto silicon wafers and then allowed to dry under ambient conditions (Entry 1~4 in Table 1). The micelle and SCK solutions were then adjusted to pH 12 and deposited onto silicon wafers (Entry 5~8). Further, the inverted micelle and SCK solutions at pH 12 were adjusted back to pH 2 and again deposited onto silicon wafers (Entry 9~12). The XPS spectra indicated that the samples contained the expected elements: Na, Cl, C, O, N and B (Figures S4 and S5). Because the escape depth of the electrons measured in XPS is only on the order of ~10 nm, the surface composition of the samples, *i.e.* the shell, was preferentially sampled and, therefore, contributed to the XPS signal more significantly than did the core. Atomic concentrations were calculated from the integrated areas under the B 1s and N 1s peaks (observed at binding energies of 191 eV and 400 eV, respectively) and their relative sensitivity factors, and nitrogen to boron (N/B) atomic ratios are shown in Table 1. The N/B ratio of non-cross-linked micelles changed dramatically from 11.7 (Entry 1) to 3.6 (Entry 5) upon pH change from 2 to 12, which indicated that the nitrogen-rich shell chains moved into the core and the boron-rich core domain solvated and shifted from the core to the shell. After adding 0.1 M HCl to return the pH to 2, the N/B ratio of the micelles reverted back to 10.3 (Entry 9). However, in 2% czaSCKs, the cyclic change of pH (2 to 12 to 2) gave N/B ratio change from 7.9 to 5.0 to 6.3 respectively. The N/B ratio changes and reversibility of 2% SCKs were less than that of the non-cross-linked micelles, which indicated that the shell cross-linking inhibited chain reptation of the PAPBA from the core to the surface and back to the core of the nanoparticles. Moreover, the N/B ratio of czaSCKs with 5% and 10% cross-linking densities showed decreasing reversibility compared to the 2% SCKs and non-cross-linked micelles.

Experimental

Materials

N,N-dimethylformamide (DMF), diethyl ether, dichloromethane (DCM), tetrahydrofuran (THF), triethylamine (TEA), 3-aminophenylboronic acid monohydrate (98%), 2,2′-azobis(isobutyronitrile) (AIBN, 98%), *N*-boc-ethylenediamine (98%), N-hydroxybenzotriazole (HOBt, 98%), 2-(1H-benzotriazole-1-yl)-1, 1, 3, 3-tetramethylaminium hexafluorophosphate (HBTU, 98%), trifluoro acetic acid (TFA, 99%) and methanol were purchased from Sigma-Aldrich Company. Acryloyl chloride (96%, stab

with 400 ppm phenothiazine) was used as received from Alfa Aesar. Nanopure water (18 MΩ·cm) was acquired by means of a Milli-Q water filtration system, Millipore Corp. (Bedford, MA). AIBN was recrystallized by methanol twice before use. All other chemicals were used without further purification, unless otherwise noted.

Instrumentation

^{1}H and ^{13}C NMR spectra were recorded on Varian 300 spectrometers. Chemical shifts were referenced to solvent resonance signals, or trimethylsilyl propanoic acid-d_4 (TSP) was used as an internal standard. IR spectra were recorded on an IR Prestige 21 system (Shimadzu Corp., Japan) and analyzed using IRsolution v. 1.40 software.

N,N-dimethylformamide-based gel permeation chromatography (DMF GPC) was conducted on a Waters Chromatography, Inc. (Milford, MA) system equipped with an isocratic pump model 1515, a differential refractometer model 2414 and a two-column set of Styragel HR 4 and HR 4E 5 mm DMF 7.8 × 300 mm columns. The system was equilibrated at 70 °C in pre-filtered DMF containing 0.05 M LiBr, which served as polymer solvent and eluent (flow rate set to 1.00 mL/min). Polymer solutions were prepared at concentrations of *ca.* 3 mg/mL and an injection volume of 0.2 mL was used. Data collection and analysis was performed with Empower Pro software. The system was calibrated with poly(ethylene glycol) standards (Polymer Laboratories, Amherst, MA) ranging from 615 to 442,800 Da.

Glass transition temperatures (T_g) were measured by differential scanning calorimetry on a Mettler-Toledo DSC822R (Mettler-Toledo, Inc., Columbus, OH), with a heating rate of 10 °C /min. Measurements were analyzed using Mettler-Toledo Star v. 7.01 software. The T_g was taken as the midpoint of the inflection tangent, upon the third heating scan. Thermogravimetric analysis (TGA) was performed under N_2 atmosphere using a Mettler-Toledo model TGA/SDTA851e, with a heating rate of 10 °C/min. Measurements were analyzed by using Mettler-Toledo Star v. 7.01 software.

Transmission electron microscopy (TEM) was conducted on a Hitachi H-7500 microscope, operating at 100 kV. Alternatively, specimens were observed on a JEOL 1200EX transmission electron microscope operating at 100 kV and micrographs were recorded at calibrated magnifications using an SIA-15C CCD camera. The final pixel size was 0.42 nm/pixel. Samples for TEM measurements were prepared as follows: 4 μL of the dilute solution (with a polymer concentration of 0.1 mg/mL) was deposited onto a carbon-coated copper grid, and after 2 min, the excess of the solution was quickly wicked away by a piece of filter paper. The samples were then negatively stained with 1 wt.% phosphotungstic acid (PTA) aqueous solution or 1 wt % uranyl acetate aqueous solution. After 1 min, the excess staining solution was quickly wicked away by a piece of filter paper and the samples were left to dry under ambient conditions overnight. Atomic force microscopy (AFM) imaging was performed using a MFP-3D system (Asylum Research, Santa Barbara, CA) in tapping mode using standard tips (Vista Probes, T190-25; length (L), 225 μm, normal spring constant, 48 N/m; resonance frequency, 190 kHz). The samples as aqueous solutions (5 μL) were deposited onto freshly-cleaved mica and allowed to dry under ambient condition before analyses. The average height and diameter values were determined by section analysis, using the IGOR Pro software package.

Hydrodynamic diameters (D_h) and size distributions for the nanoparticles in aqueous solutions were determined by dynamic light scattering (DLS). The DLS instrumentation consisted of a Brookhaven Instruments Limited (Worcestershire, U.K.) system, including a model BI-200SM goniometer, a model BI-9000AT digital correlator, a model EMI-9865 photomultiplier, and a model 95-2 Ar ion laser (Lexel Corp.) operated at 514.5 nm. Measurements were made at 25 ± 1 °C. Scattered light was collected at a fixed angle of 90°.

The digital correlator was operated with 522 ratio spaced channels, and initial delay of 5 μs, a final delay of 100 ms, and a duration of 2 minutes. A photomulitplier aperture of 100 μm was used, and the incident laser intensity was adjusted to obtain a photon counting of between, 200 and 300 kcps. Only measurements in which the measured and calculated baselines of the intensity autocorrelation function agreed to within 0.1 % were used to calculate particle size. The calculations of the particle size distributions and distribution averages were performed with the ISDA software package (Brookhaven Instruments Company), which employed single-exponential fitting, cumulants analysis, and CONTIN particle size distribution analysis routines. Alternatively, DLS measurements were also conducted using a Delsa Nano C from Beckman Coulter, Inc. (Fullerton, CA) equipped with a laser diode operating at 658 nm. Size measurements were made in nanopure water. Scattered light was detected at 165° angle and analyzed using a log correlator over 70 accumulations for a 0.5 mL sample in a glass size cell (0.9 mL capacity). The photomultiplier aperture and the attenuator were automatically adjusted to obtain a photon counting rate of *ca*. 10 kcps. Calculation of the particle size distribution and distribution averages was performed using CONTIN particle size distribution analysis routines using Delsa Nano 2.31 software. The peak averages of histograms from intensity, volume and number distributions out of 70 accumulations were reported as the average diameter of the particles. All determinations were repeated 5 times.

The particle zeta potentials were determined by a Delsa Nano C particle analyzer (Beckman Coulter. Fullerton, CA) equipped with a 30 mW dual laser diode (658 nm). The zeta potential of the particles in suspension was obtained by measuring the electrophoretic movement of charged particles under an applied electric field. Scattered light was detected at a 30° angle at 25 °C. In each measurement, NaCl solution was added to adjust the sample to 10 mM. The zeta potential was measured at five regions in the flow cell and a weighted mean was calculated. These five measurements were used to correct for electroosmotic flow that was induced in the cell due to the surface charge of the cell wall. All determinations were repeated 5 times.

A potentiometric titration of homopolymer PAEA was performed at room temperature using an automatic titrator system (HI902C, Hanna Instruments, USA) equipped with a pH electrode (Glass electrode HI1131, Hanna Instruments, USA). The calibration of the electrode was carried out using buffer solutions (pH 4.01, pH 7.01 and pH 10.01, Hanna Instruments, USA). Samples were prepared by dissolving 20 mg of polymer in 50 mL of freshly prepared 0.01 N NaOH solution (150 mM NaCl). The titrant (0.01N HCl, 150 mM NaCl) was added in 0.05 mL portions at 5–60 s intervals when the drift equilibrium reached the rate of 1 mV/s.

XPS spectra were obtained with a Kratos Axis Ultra DLD spectrometer with a monochromatic Al Ka source operated at 150 W. Survey spectra and high resolution elemental scans were obtained at pass energies of 80 eV and 20 eV, respectively. Charge neutralization was used to compensate for charging effects, and all spectra were then corrected to C 1s at 284.6 eV.

Synthesis of (3-acrylamidophenyl)boronic acid 2—In a 250 mL round-bottom flask equipped with a magnetic stir bar 3-aminophenylboronic acid monohydrate (3.16 g, 20 mmol) was dissolved in a 1:1 mixture of THF (40 mL) and water (40 mL). Sodium bicarbonate (3.36 g, 40 mmol) and acryloyl chloride (3.77 g, 40 mmol) were added to the flask at 0~5 °C. The solution was stirred for 4 h and the THF was subsequently removed *in vacuo*. A solid crude product was obtained and stirred in ethyl acetate (50 mL) for 2 h. After filtering the solid materials, the organic layer was washed with water (50 mL), saturated sodium bicarbonate solution (50 mL), water (50 mL) and brine (50 mL), respectively. The

organic layer was dried over $MgSO_4$. Concentration *in vacuo* of the organic phase yielded **2** as a white solid. The crude product was collected and recrystallized from hot water twice to give white plate-like crystals (2.61 g, 68 % yield). ^{1}H NMR (300 MHz, DMSO-d_6, ppm): δ 5.71–5.75 (dd, 1H, J = 10 Hz and J = 2 Hz, vinyl C*H*), 6.22–6.29 (dd, 1H, J = 17 Hz and J = 10 Hz, vinyl C*H*), 6.42–6.51 (dd, 1H, J = 17 Hz and J = 2 Hz, vinyl C*H*), 7.27–7.90 (m, 4H, Ar*H*), 8.00 (br, 2H, $B(OH)_2$). ^{13}C NMR (75 MHz, DMSO-d_6, ppm): δ 121.9, 125.9, 127.1, 128.3, 129.9, 132.5, 134.3 138.7, 163.6. FT-IR (cm^{-1}): 3650-3050, 1659, 1551, 1427, 1342, 1250, 1157, 1088, 1011, 949, 903, 825, 790. HRMS: calculated $[M+H]^+$ for $C_9H_{10}BNO_3$: 192.0832 Da, found: 192.0830 Da.

Synthesis of tert-butyl (2-acrylamidoethyl)carbamate 5—To a solution of *N*-Boc-ethylenediamine (3.85 g, 24 mmol) in DCM (20 mL) at 0 °C, TEA (3.64 g, 36 mmol) was added. Acryloyl chloride (2.26 g, 24 mmol) in DCM (5 mL) was then added dropwise over 10 min. The reaction mixture was stirred at 0 °C for 3 h and then kept at 0–5 °C for another 21 h. The reaction mixture was filtered and the residue was washed by DCM (20 mL). The filtrate was washed by water (50 mL) and brine (50 mL), respectively, and then dried over $MgSO_4$. Concentration *in vacuo* of the organic phase yielded **5** as a white solid. The crude product was collected and recrystallized from ethyl acetate twice to give a white solid (3.14 g, 61 % yield). ^{1}H NMR (300 MHz, $CDCl_3$, ppm): δ 1.43 (s, 9H, 3 × CH_3), 3.30–3.45 (m, 4H, NHCH_2CH_2NH), 4.94 (br, 1H, N*H*-Boc), 5.61–5.65 (dd, 1H, J = 11 Hz and J = 2 Hz, vinyl C*H*), 6.05–6.14 (dd, 1H, J = 17 Hz and J = 11 Hz, vinyl C*H*), 6.23–6.29 (dd, 1H, J = 17 Hz and J = 2 Hz, vinyl C*H*), 6.48 (br, 1H, CON*H*CH_2CH_2). ^{13}C NMR (75 MHz, $CDCl_3$, ppm): δ 28.4, 40.1, 40.9, 79.7, 126.3, 130.9, 157.1, 166.3. FT-IR (cm^{-1}): 3400-3150, 3078, 2978, 1668, 1543, 1412, 1280, 1242, 1165, 979, 864. HRMS: calculated $[M+H]^+$ for $C_{10}H_{18}N_2O_3$: 216.1474 Da, found: 216.1482 Da.

Synthesis of $PAPBA_{30}$ 3—In a 10 mL Schlenk flask equipped with a magnetic stir bar, DDMAT **4** (29 mg, 0.079 mmol, 1 eq), (3-acrylamidophenyl)boronic acid (754 mg, 3.95 mmol, 50 eq) and AIBN (1.72 mg, 0.0158 mmol, 0.2 eq) were added and dissolved in DMF/H_2O mixed solvent (v/v = 95/5, 7 mL). The reaction mixture was deoxygenated by freeze-pump-thaw (3×) and then placed in a preheated reaction bath at 70 °C. The polymerization was quenched after 7 h by removing the polymerization flask from the heating bath and cooling with liquid nitrogen. The resulting mixture was poured into cold ether (40 mL) and the precipitate was collected by filtration. The precipitate was dried under vacuum to give **3** as a yellow solid (442 mg, 79 % yield, based on 70 % conversion). M_n^{NMR} = 6.2 kDa, DP_n = 30, (pinacol protected polymer: M_n^{GPC} = 13.7 kDa, PDI^{GPC} = 1.08). ^{1}H NMR (300 MHz, DMSO-d_6 with one drop of D_2O, ppm): δ 0.82 (m, 3H, CH_3), 1.11–1.33 (br, 10 × CH_2 from **4**), 1.39–2.11 (br, PAPBA backbone protons and 2 × CH_3 from **4**), 6.76–8.00 (br, Ar*H*), 9.55 (br, OCN*H*Ar). ^{13}C NMR (75 MHz, DMSO-d_6 with one drop of D_2O, ppm): δ 28.3–28.8 (multiple peaks), 43.1, 122.9, 126.5, 127.8, 129.4, 134.5, 138.5, 162.9. FT-IR (cm^{-1}): 3650-3050, 2931, 1651, 1543, 1427, 1327, 1157, 1096, 1049, 902. (T_g) = 71 °C. TGA in N_2: 0–200 °C, 13% mass loss; 200–320 °C, 8% mass loss; 320–450 °C, 36% mass loss, 43% mass remaining above 600 °C.

Synthesis of $PAPBA_{30}$-b-$PAEANBoc_{25}$ 6—In a 10 mL Schlenk flask equipped with a magnetic stir bar, $PAPBA_{30}$ **3** (290 mg, 0.0468 mmol, 1 eq), *tert*-butyl (2-acrylamidoethyl)carbamate (501 mg, 2.339 mmol, 50 eq) and AIBN (1.5 mg, 0.00936 mmol, 0.2 eq) were added and dissolved in DMF/H_2O mixed solvent (v/v = 98/2, 8 mL). The reaction mixture was deoxygenated by freeze-pump-thaw (3×) and then placed in a preheated reaction bath at 70 °C. The polymerization was quenched after 8 h by removing the polymerization flask from the heating bath and cooling with liquid nitrogen. The resulting mixture was poured into cold ether (40 mL) and the precipitate was collected by

centrifugation. The precipitate was dried under vacuum to give **6** as a pale yellow solid (520 mg, 85 % yield, based on 65% conversion). M_n^{NMR} = 11.6 kDa, $(DP_n)_{PAEANBoc}$ = 25, (pinacol protected polymer: M_n^{GPC} = 26.7 kDa, PDI^{GPC} = 1.10). ^{1}H NMR (300 MHz, DMSO-d_6 with one drop of D_2O, ppm): δ 0.82 (m, 3H, CH_3), 1.08–1.45 (br, 3 × CH_3 from Boc and protons from **4**), 1.45–2.25 (br, polymer backbone protons), 2.43–3.25 (br, CONHCH_2CH_2NCOOCCH_3), 6.63–7.93 (br, ArH), 9.55 (br, OCNHAr). ^{13}C NMR (75 MHz, DMSO-d_6 with one drop of D_2O, ppm): δ 28.3–28.8 (multiple peaks), 31.3, 36.3, 78.3, 123.0, 126.4–129.5, 156.2, 157.3, 163.0, 173.6. (T_g) = 69 °C and 160 °C. TGA in N_2: 0–250 °C, 28% mass loss; 250–260 °C, 24% mass loss; 260–420 °C, 19% mass loss, 29% mass remaining above 600 °C.

Synthesis of PAPBA$_{30}$-b-PAEA$_{25}$ 1—In a 5 mL round-bottom flask equipped with a magnetic stir bar, diblock copolymer PAPBA$_{30}$-*b*-PNBoc$_{25}$ **6** (320 mg, 0.0276 mmol) was suspended in TFA (2 mL). The reaction mixture was then stirred at room temperature for 5 h. The mixture was purified by dialysis against nanopure water for 2 d by using dialysis membrane (MWCO = 8000 Da). The resulting solution was lyophilized to give **1** as a white solid (240 mg, 73% yield). ^{1}H NMR (300 MHz, DMSO-d_6 with one drop of D_2O, ppm): δ 0.80–2.43 (br, polymer backbone protons and protons form CTA), 2.78–3.68 (br, CONHCH_2CH_2NH_2), 6.83–8.59 (br, ArH and OCNHCH_2), 9.55 (br, OCNHAr). ^{13}C NMR (75 MHz, DMSO-d_6 with one drop of D_2O, ppm): δ 39.2–44.2 (multiple overlapping br), 122.8, 126.3, 127.9, 129.4, 134.5, 138.4, 162.8, 175.5. FT-IR (cm^{-1}): 3600-3250, 3071, 2932, 1659, 1543, 1435, 1342, 1141, 795. DSC: (T_g) = 72 °C and 176 °C. TGA in N_2: 120–200 °C, 4% mass loss; 200–240 °C, 15% mass loss; 240–360 °C, 12% mass loss, 360–460 °C, 15% mass loss, 54% mass remaining above 600 °C.

Typical procedure to prepare micelles and czaSCKs

To a 20 mL vial was added PAPBA$_{30}$-*b*-PAEA$_{25}$ **1** (10 mg) and nanopure water (5 mL, pH 5.5). The mixture was sonicated at room temperature for 5 min to form a bluish-colored micelle solution. To crosslink the micelles (2% cross-linking density for example), the diacid crosslinker (0.057 mg, 0.17 μmol) was activated by mixing with 3 equiv. of HOBt/HBTU (0.08 mg/0.21 mg, 1:1, mol:mol) in DMF (100 μL) and allowed to stir for 1 h. This solution was then added with stirring to the micelle solution, which had undergone adjustment of the pH to 7.0, using 0.1 M aqueous NaOH. The reaction mixture was allowed to stir for 2 d at r.t, and then transferred to dialysis tubing (MWCO: 8 kDa) and dialyzed against nanopure water for 2 days. A bluish-colored solution containing czaSCKs with a final concentration of 1.5 mg/mL was obtained. The 5% and 10% crosslinked czaSCKs were prepared by similar method using stoichiometric amount of crosslinker. The czaSCKs solutions were lyophilized to give white fluffy powders. These powders can be resuspended into aqueous solution with desired pH followed by 5 min sonication to give czaSCK solutions for further characterizations.

Conclusions

In conclusion, a new type of dual boronic acid- and amino-containing well-defined diblock copolymer was synthesized by sequential RAFT polymerization and transformed into multiple stimuli-responsive nanostructures having unique morphological inversion behaviors. Assembly of the diblock copolymer into schizophrenic type micelles in water without and with covalent cross-linking reactions throughout the shell domain, giving czaSCKs, allowed for direct determination of the pH and sugar dual stimuli responsive properties, by a combination of zeta potential, TEM, AFM, DLS, NMR and XPS studies. These smart nanoparticles present strong positive surface charge at low pH and high negative surface charge at high pH. In the presence of D-glucose, the IEP dropped due to the

formation of borate-glucose complexes. The IEP value could also be tuned by different cross-linking degrees. Disassembly and reassembly events with differential micellar sizes were observed for the full, reversible inversions of the block copolymers assembled supramolecularly into micelles, whereas stabilization by the shell crosslinks was found to result in maintenance of the original multi-molecular aggregate sizes for the czaSCKs, whether at low or high pH. Moreover, reversible migration of the non-crosslinked core chain segments through the crosslinked shell was observed by NMR spectroscopy and zeta potential measurements, with XPS experiments providing quantitative determination that increasing shell cross-linking densities resulted in decreasing ability and reversibility for the presumed core chain reptation processes.

Supplementary Material

Refer to Web version on PubMed Central for supplementary material.

Acknowledgments

This work was supported in part from the National Heart Lung and Blood Institute of the National Institutes of Health as a Program of Excellence in Nanotechnology (HHSN268201000046C) and the National Science Foundation under grant numbers DMR-0906815 and DMR-1105304. The Welch Foundation is gratefully acknowledged for support through the W. T. Doherty-Welch Chair in Chemistry, Grant No. A-0001. The transmission electron microscopy facilities at Washington University in St. Louis, Department of Otolaryngology, Research Center for Auditory and Visual Studies funded by NIH P30 DC004665 were used for acquisition of some of the TEM images. The authors thank Dr. Guorong Sun for helpful discussion and Ms. Adriana Pavia for drawing schemes. Supporting Information is available online from Wiley InterScience or from the author.

Note and References

1. Alarcon CDH, Pennadam S, Alexander C. Chemical Society Reviews. 2005; 34:276–285. [PubMed: 15726163]
2. Chen DY, Jiang M. Accounts of Chemical Research. 2005; 38:494–502. [PubMed: 15966716]
3. Dimitrov I, Trzebicka B, Muller AHE, Dworak A, Tsvetanov CB. Progress in Polymer Science. 2007; 32:1275–1343.
4. Gil ES, Hudson SM. Progress in Polymer Science. 2004; 29:1173–1222.
5. Stuart MAC, Huck WTS, Genzer J, Muller M, Ober C, Stamm M, Sukhorukov GB, Szleifer I, Tsukruk VV, Urban M, Winnik F, Zauscher S, Luzinov I, Minko S. Nature Materials. 2010; 9:101–113.
6. Boyer C, Stenzel MH, Davis TP. Journal of Polymer Science Part a-Polymer Chemistry. 2011; 49:551–595.
7. Ebara M, Uto K, Idota N, Hoffman JM, Aoyagi T. Advanced Materials. 2012; 24:273–278. [PubMed: 21954058]
8. Lee NS, Sun GR, Neumann WL, Freskos JN, Shieh JJ, Dorshow RB, Wooley KL. Advanced Materials. 2009; 21:1344–1348. [PubMed: 22058610]
9. Ding ZL, Fong RB, Long CJ, Stayton PS, Hoffman AS. Nature. 2001; 411:59–62. [PubMed: 11333975]
10. Schmaljohann D. Advanced Drug Delivery Reviews. 2006; 58:1655–1670. [PubMed: 17125884]
11. Ganta S, Devalapally H, Shahiwala A, Amiji M. Journal of Controlled Release. 2008; 126:187–204. [PubMed: 18261822]
12. Jin QA, Liu GY, Ji JA. Journal of Polymer Science Part a-Polymer Chemistry. 2010; 48:2855–2861.
13. Dong L, Agarwal AK, Beebe DJ, Jiang HR. Nature. 2006; 442:551–554. [PubMed: 16885981]
14. Banerjee I, Pangule RC, Kane RS. Advanced Materials. 2011; 23:690–718. [PubMed: 20886559]
15. Liu SY, Armes SP. Angewandte Chemie-International Edition. 2002; 41:1413–1416.
16. Jiang X, Zhang G, Narain R, Liu S. Langmuir. 2009; 25:2046–2054. [PubMed: 19140708]

17. Bories-Azeau X, Armes SP, van den Haak HJW. Macromolecules. 2004; 37:2348–2352.
18. Butun V, Liu S, Weaver JVM, Bories-Azeau X, Cai Y, Armes SP. Reactive & Functional Polymers. 2006; 66:157–165.
19. Lee NS, Li YL, Ruda CM, Wooley KL. Chemical Communications. 2008:5339–5341. [PubMed: 18985203]
20. Liu FT, Eisenberg A. Journal of the American Chemical Society. 2003; 125:15059–15064. [PubMed: 14653740]
21. Rodriguez-Hernandez J, Lecommandoux S. Journal of the American Chemical Society. 2005; 127:2026–2027. [PubMed: 15713063]
22. Wooley KL. Journal of Polymer Science Part a-Polymer Chemistry. 2000; 38:1397–1407.
23. Nystrom AM, Bartels JW, Du W, Wooley KL. Journal of Polymer Science Part a-Polymer Chemistry. 2009; 47:1023–1037.
24. Ding ZL, He WD, Tao J, Jiang WX, Li LY, Pan TT. Journal of Polymer Science Part a-Polymer Chemistry. 2011; 49:2783–2789.
25. Butun V, Top RB, Ufuklar S. Macromolecules. 2006; 39:1216–1225.
26. Wang D, Liu T, Yin J, Liu SY. Macromolecules. 2011; 44:2282–2290.
27. Matsumoto A, Yoshida R, Kataoka K. Biomacromolecules. 2004; 5:1038–1045. [PubMed: 15132698]
28. Martin C, Ronda JC, Cadiz V. Polymer Degradation and Stability. 2006; 91:747–754.
29. Roy D, Cambre JN, Sumerlin BS. Chemical Communications. 2008:2477–2479. [PubMed: 18491020]
30. Roy D, Cambre JN, Sumerlin BS. Chemical Communications. 2009:2106–2108. [PubMed: 19360161]
31. Bapat AP, Roy D, Ray JG, Savin DA, Sumerlin BS. Journal of the American Chemical Society. 2011; 133:19832–19838. [PubMed: 22103352]
32. Kudaibergenov SE, Ciferri A. Macromolecular Rapid Communications. 2007; 28:1969–1986.
33. Armitage P, Ebdon JR, Hunt BJ, Jones MS, Thorpe FG. Polymer Degradation and Stability. 1996; 54:387–393.
34. Qin Y, Cheng GL, Sundararaman A, Jakle F. Journal of the American Chemical Society. 2002; 124:12672–12673. [PubMed: 12392409]
35. Qin Y, Cui CZ, Jakle F. Macromolecules. 2007; 40:1413–1420.
36. Cambre JN, Roy D, Gondi SR, Sumerlin BS. Journal of the American Chemical Society. 2007; 129:10348–10349. [PubMed: 17676853]

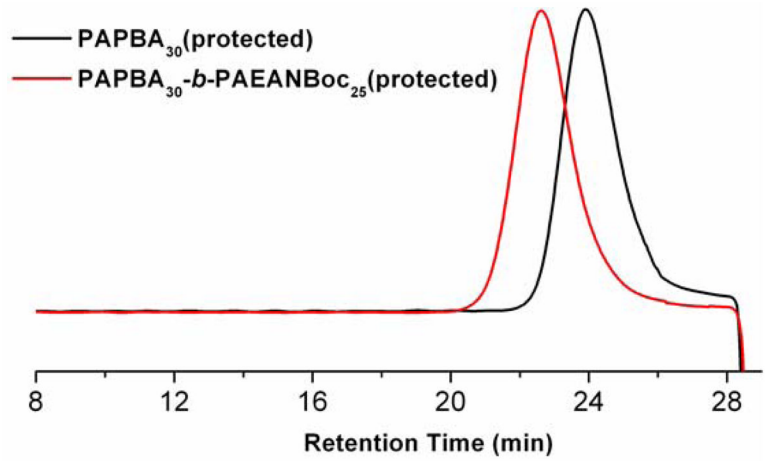

Fig. 1.
GPC traces of pinacol-protected $PAPBA_{30}$, **3**, and $PAPBA_{30}$-*b*-$PAEANBoc_{25}$, **6**.

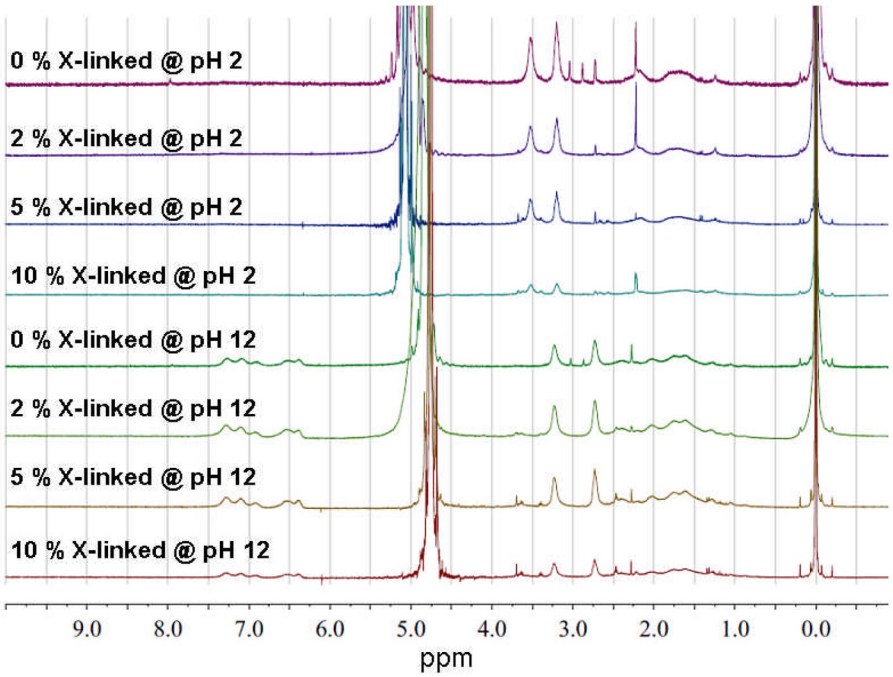

Fig. 2.

^{1}H NMR spectra (300 MHz, D_2O) of $PAPBA_{30}$-*b*-$PAEA_{25}$, **1**, as amphiphilic micellar assemblies and czaSCKs at 2%, 5% and 10% cross-linking density at pH 2 (upper four spectra) and at pH 12 (lower four spectra). Trimethylsilyl propanoic acid-d_4 (TSP) was used as an internal standard.

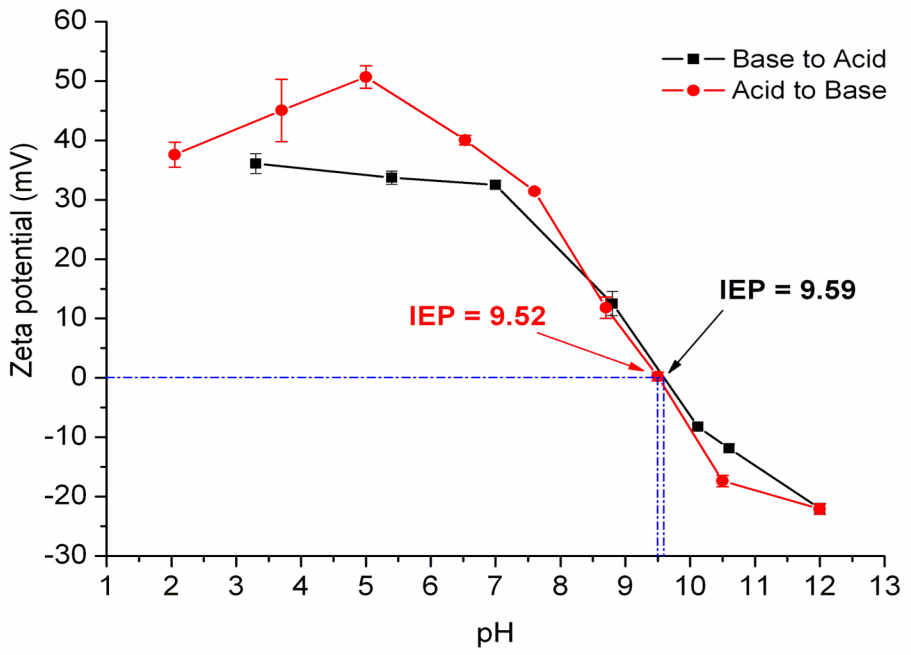

Fig. 3.

Zeta potential changes of micelles as a function of pH, for samples having the pH adjusted from acidic to basic (red circles) and basic to acidic (black squares). Error bars represent standard deviations of 5 runs. The pH change of each data point during the measurements was less than ± 0.1.

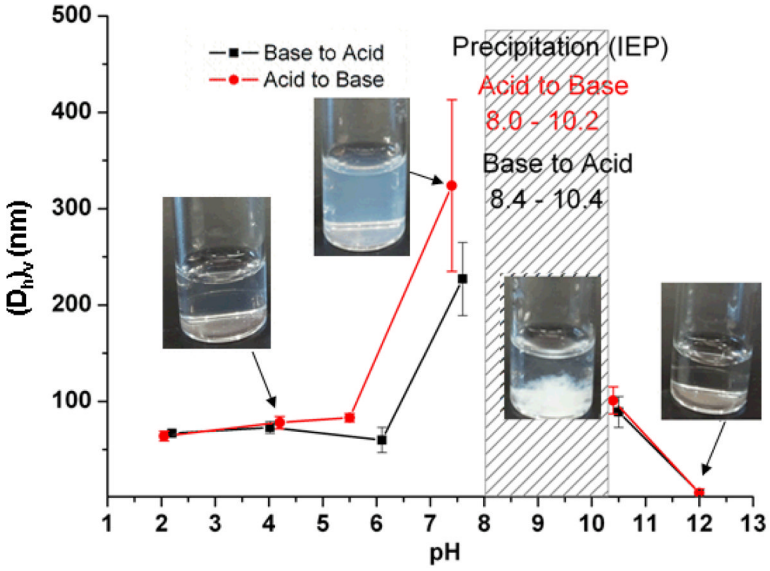

Fig. 4.

Volume-based hydrodynamic diameter $(D_h)_v$ change as a function of pH. Error bars represent standard deviations of 5 runs. The pH change of each data point during the measurements was less than ± 0.1.

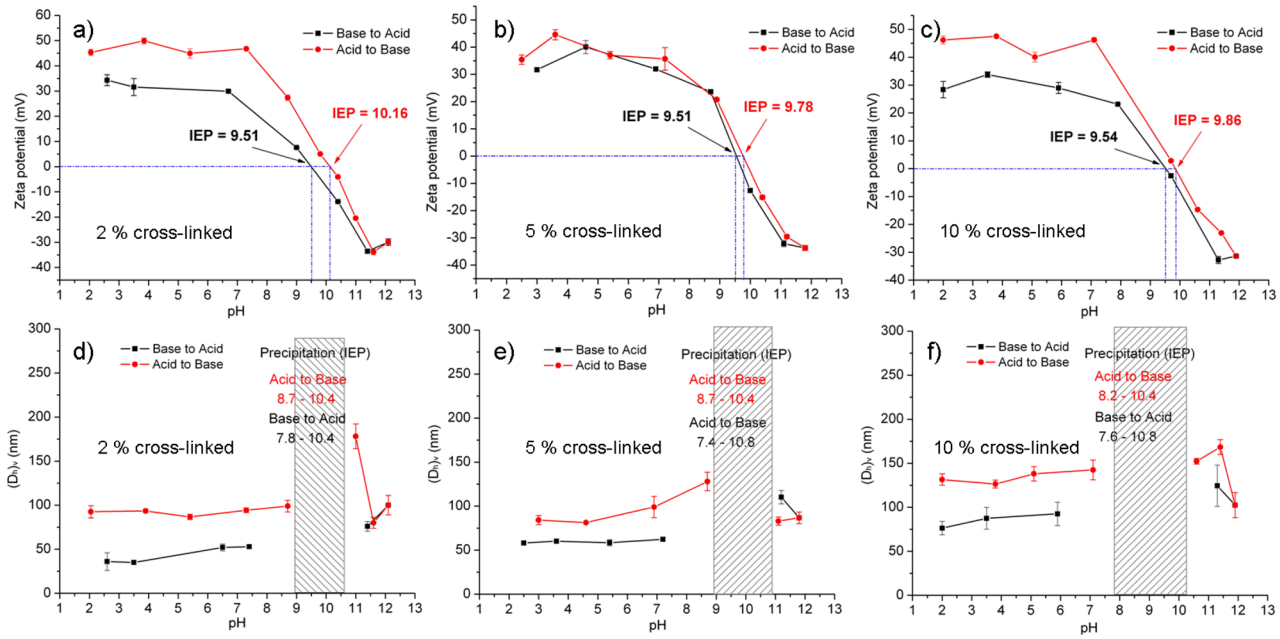

Fig. 5.

Zeta potential and $(D_h)_v$ changes for czaSCKs at 2%, 5% and 10% cross-linking densities as a function of pH. Error bars represent standard deviations of 5 runs. The pH change of each data point during the measurements was less than ± 0.1.

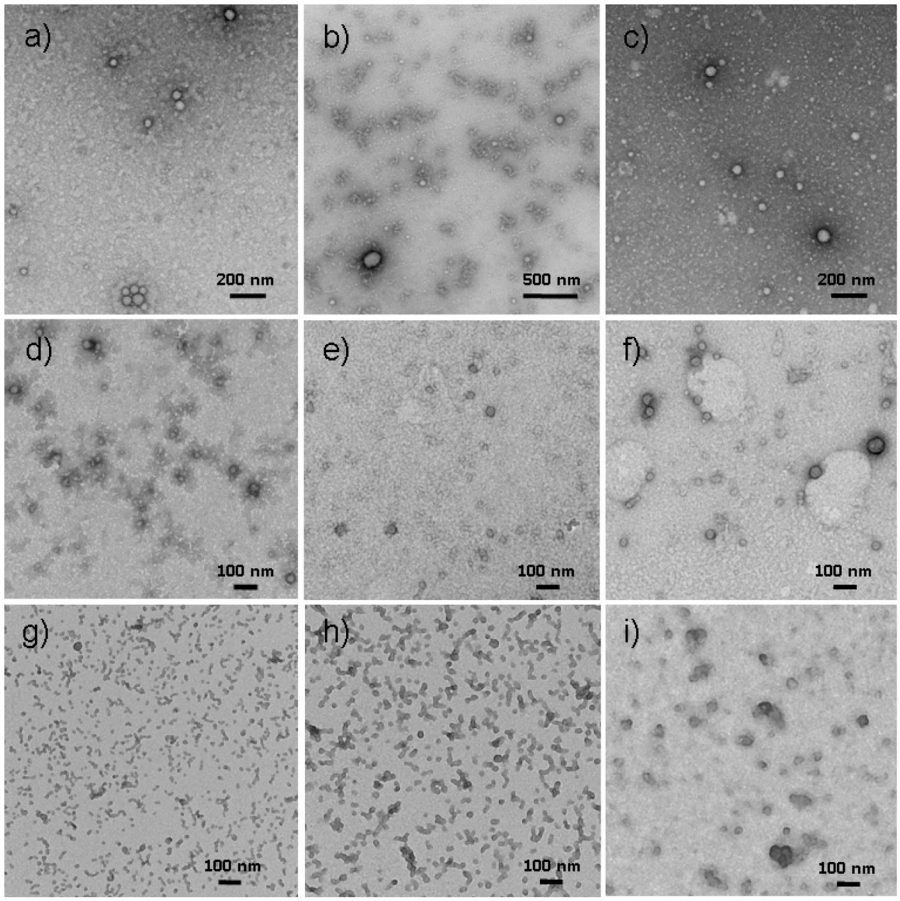

Fig. 6.

TEM images for non-cross-linked micelles and czaSCKs deposited from aqueous solutions at different pH values onto carbon-coated copper grids and allowed to dry under ambient conditions: a) non-cross-linked micelles at pH 2; b) non-cross-linked micelles at pH 7.3; c) non-cross-linked micelles at pH 10.5; d) 2% cross-linked czaSCKs at pH 2; e) 5% cross-linked czaSCKs at pH 2; f) 10% cross-linked czaSCKs at pH 2; g) 2% cross-linked czaSCKs at pH 12; h) 5% cross-linked czaSCKs at pH 12; i) 10% cross-linked czaSCKs at pH 12. Samples imaged as a,b,c,e,f,g,h were negatively stained by uranyl acetate; d and i were stained by phosphotungstic acid.

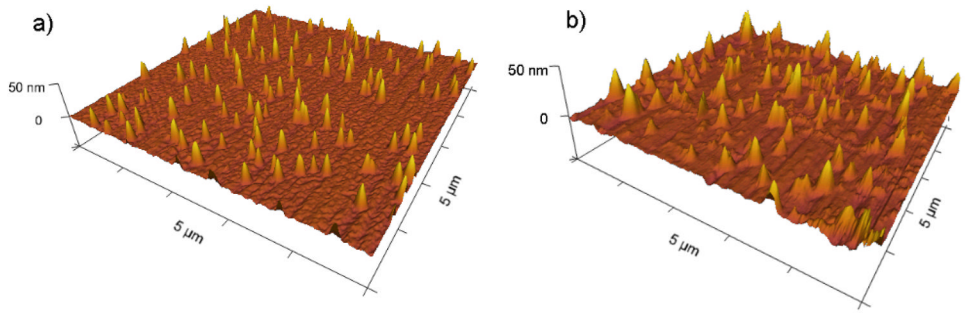

Fig. 7.

Tapping-mode AFM images for 10 % czaSCKs drop deposited from aqueous solutions at pH 2 a) and pH 12 b) onto freshly-cleaved mica and allowed to dry under ambient conditions.

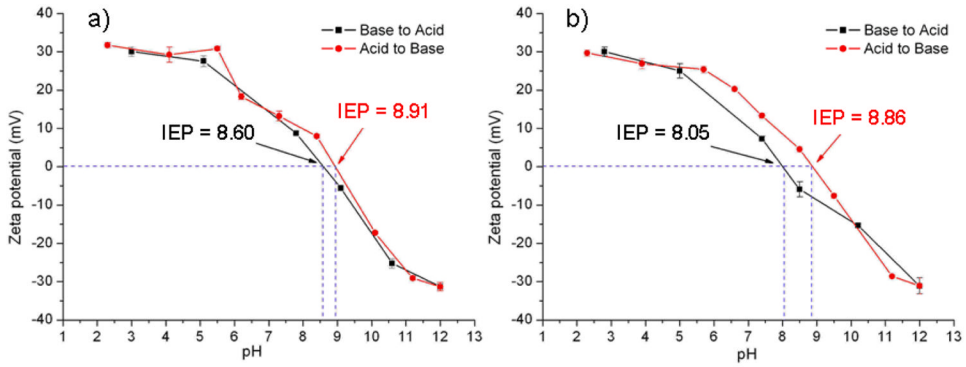

Fig. 8.

Zeta potential changes of non-cross-linked micelles as a function of pH with a) 5 eq of D-glucose; b) 15 eq of D-glucose.

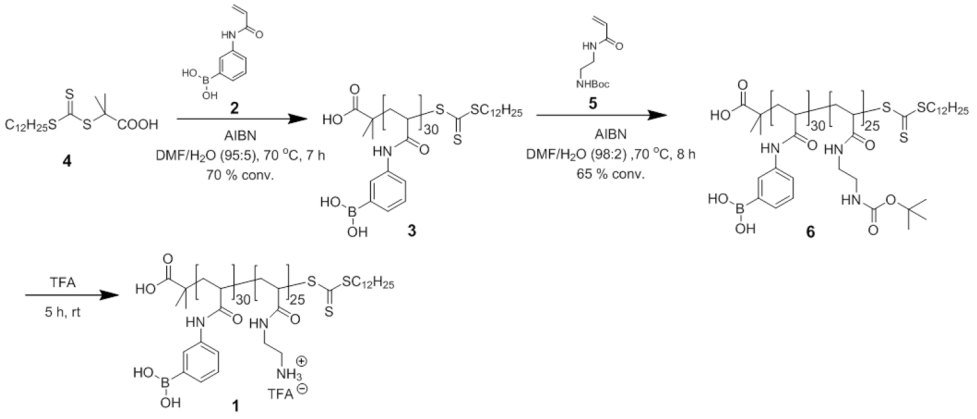

Scheme 1.
Synthesis of $PAPBA_{30}$-*b*-$PAEA_{25}$ by sequential RAFT polymerizations and acidolysis.

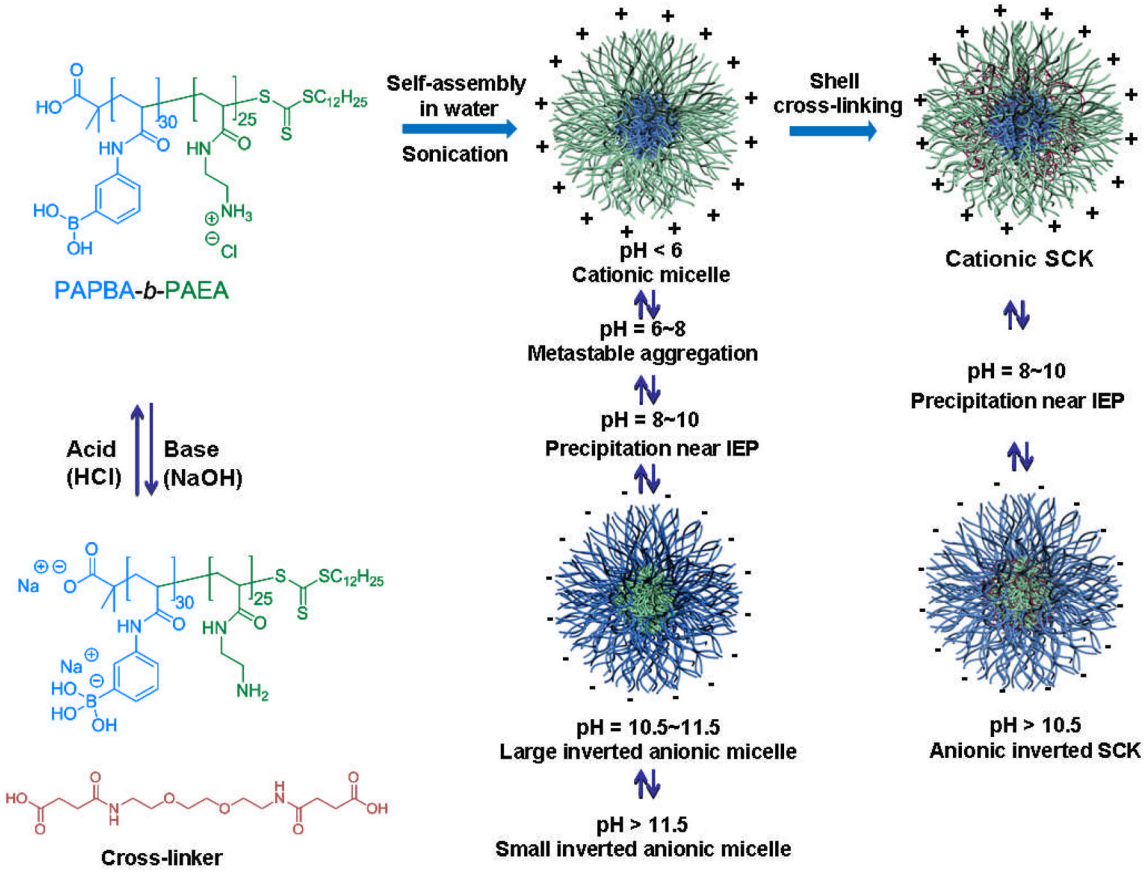

Scheme 2.
pH-triggered reversible morphology and charge inversion of micelles and SCKs.

Table 1

Elemental analysis of non-cross-linked micelles, czaSCKs (2%, 5% and 10%) at pH 2 and pH 12 by XPS.

Entry	Entry	N 1s Atomic Conc (%)	B 1s Atomic Conc (%)	N/B ratio[a]
1	Non-cross-linked micelles (pH 2)	12.97	1.11	11.7
2	2% czaSCK (pH 2)	11.43	1.44	7.9
3	5% czaSCK (pH 2)	11.38	1.24	9.2
4	10% czaSCK (pH 2)	11.20	1.07	10.5
5	Non-cross-linked micelles (pH 12)	3.70	1.03	3.6
6	2% czaSCK (pH 12)	6.04	1.20	5.0
7	5% czaSCK (pH 12)	3.07	0.49	6.3
8	10% czaSCK (pH 12)	7.16	0.70	10.2
9	Non-cross-linked micelles (pH 2)	10.40	1.01	10.3
10	2% czaSCK (pH 2)	9.25	1.48	6.3
11	5% czaSCK (pH 2)	8.57	1.67	5.1
12	10% czaSCK (pH 2)	8.67	0.96	9.0